Coastal Engineering 171 (2022) 104047

Contents lists available at ScienceDirect

Coastal Engineering

journal homepage: www.elsevier.com/locate/coastaleng

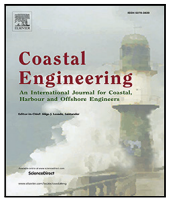

The wave overtopping load on landward slopes of grass-covered flood defences: Deriving practical formulations using a numerical model

Vera M. van Bergeijk *, Jord J. Warmink, Suzanne J.M.H. Hulscher

Department of Marine and Fluvial Systems, University of Twente, Drienerlolaan 5, Enschede, 7522 NB, The Netherlands

ARTICLE INFO

Keywords:
Hydraulic forces
OpenFOAM
Erosion
Grass failure
Levee
Wave impact

ABSTRACT

Overtopping waves exert a high hydraulic load on the landward slopes of flood defences leading to erosion of the grass cover and finally to a dike breach. The hydraulic load is an important variable in erosion models and a detailed description of the load is necessary to determine where and when the grass cover erodes. We use a numerical model to simulate the flow of a single overtopping event over a flood defence with a grass-covered crest and landward slope. The model results show that the flow velocity, the shear stress and the pressure are maximal at the landward toe and can be used to describe grass erosion by shear forces. For steep slopes, the flow separates at the crest line and impacts on the upper slope. The normal stress is maximal at the location of impact and describes the grass erosion by normal forces. Practical formulations are developed for the maximum flow velocity, the maximum pressure, the maximum shear stress, the maximum normal stress and the impact location using three main design parameters for the landward slope: the overtopping volume, the slope steepness and the slope length. The formulations are able to accurately predict the overtopping load with Nash–Sutcliffe model efficiency factors between 0.41 and 0.90. The model output and these new formulations are used to calculate the erosive power of the overtopping waves predicted by eight erosion indices to show how the simulated load can be used in erosion models.

1. Introduction

Grass-covered earthen flood defences are widely used to protect coastal and fluvial areas from flooding. Numerous flood defences need to be strengthened in the coming decades due to new design rules and new insights in the failure process (Slomp et al., 2016). Moreover, sea level rise and increasing river discharges can lead to higher design water levels (Toimil et al., 2020; Blöschl et al., 2019). Additionally, drier summers are expected as the result of climate change reducing the strength of both the dike cover and core of flood defences (Norton et al., 2016; Bottema et al., 2021).

One of the main failure mechanisms of these types of flood defences is grass cover erosion by wave overtopping. Waves flow over the dike crest and accelerate along the landward slope resulting in high turbulent flow velocities with large erosive power. Wave overtopping experiments on grass-covered dikes show three main locations of erosion: (1) transitions, (2) the landward toe and (3) the upper landward slope (Van der Meer, 2008; Van der Meer et al., 2010; Steendam et al., 2014; Van Damme et al., 2016). Firstly, roughness transitions can create additional turbulence, objects on the dike lead to flow concentration and height transitions can lead to flow separation and impact, which all increase the erosive power (Van Hoven et al., 2013; Bomers et al., 2018; Van Bergeijk et al., 2021). Erosion at the landward toe is the result of high flow velocities at the end of the slope in combination with the slope change resulting in an additional impact (Warmink et al., 2020; Van Bergeijk et al., 2020a) (Fig. 1b). In case of steep slopes, the overtopping flow can separate from the dike profile at the crest line and reattaches on the slope where this impact leads to a high load on the upper slope (Ponsioen et al., 2019) (Fig. 1a).

The individual overtopping waves result in an instantaneous turbulent flow leading to a higher hydraulic load compared to overflow. Multiple hydrodynamic variables are used to calculate the load by overtopping waves which can be separated in two loading mechanisms: shear forces pulling horizontally on the cover and normal forces pulling perpendicular to the cover. The shearing forces are calculated using the flow velocity (Hoffmans, 2012; Van der Meer et al., 2010; Van Bergeijk et al., 2021), the shear stress (Hoffmans, 2012; Bomers et al., 2018; Aguilar-López et al., 2018) and the work (Dean et al., 2010) or the excess wave volume (Hughes, 2011). The normal stress (Ponsioen et al., 2019) and pressure are used to describe the normal forces (Van Bergeijk et al., 2020b) that lead to failure in case of wave impact (Fig. 1a). However, it is not known under which conditions impact occurs and

* Corresponding author.
E-mail address: v.m.vanbergeijk@utwente.nl (V.M. van Bergeijk).

https://doi.org/10.1016/j.coastaleng.2021.104047
Received 15 July 2021; Received in revised form 3 October 2021; Accepted 30 October 2021
Available online 11 November 2021

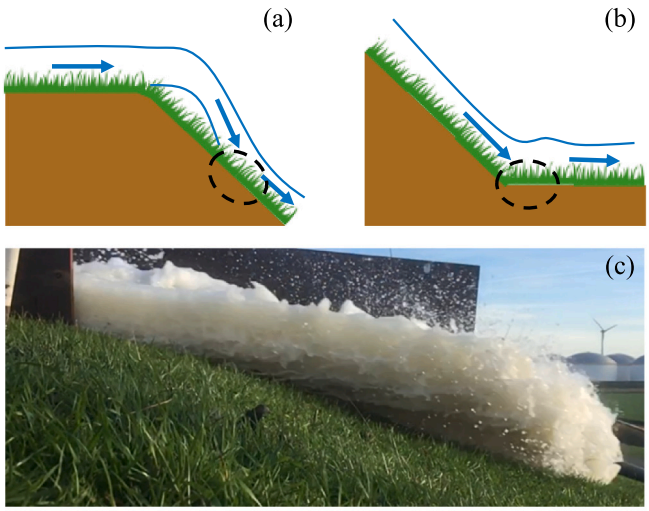

Fig. 1. Schematisation of the location of maximum load indicated by the black dashed circle. (a) Flow separation at the crest line leads to a high hydraulic load at the location of reattachment. (b) High hydraulic load at the landward toe due to high flow velocities in combination with the slope change. (c) Photo of flow separation at the crest line. Made by Rik Wegman.

therefore it remains unclear what the main loading mechanism is for specific flood defences.

Several empirical and analytical models are available to describe the load by overtopping waves in erosion models such as the cumulative overload method (Van der Meer et al., 2010), the analytical grass-erosion model (Van Bergeijk et al., 2021) and the wave impact method (Ponsioen et al., 2019). The maximum flow velocity is a frequently used variable to describe the overtopping load because it is easy to measure during experiments and it is used to describe the erosion during overflow as well. However, the maximum flow velocity does not take the effect of turbulence into account and therefore a multiplication factor is necessary to describe the load at transitions (Van der Meer et al., 2010; Warmink et al., 2020; Hoffmans et al., 2018). Multiple formulas are available for the maximum flow velocity on the crest as function of the overtopping volume as well as the acceleration along the landward slope, which may be used to determine the location and the value of the maximum flow velocity (Van der Meer et al., 2010; Van Bergeijk et al., 2019b). These formulas are likewise used in shear stress based erosion models (Hoffmans, 2012), the work method (Dean et al., 2010) and the excess volume method (Hughes, 2011) where the load is related to the second or third power of the flow velocity. Ponsioen et al. (2019) developed an analytical approach for the normal stress due to wave impact based on the flow velocity, while no calculations methods for the pressure by overtopping waves exist yet. The main problem is that the variations in time and due to turbulence are not explicitly included in these empirical and analytical models, while the instantaneous turbulent nature of the overtopping waves is one of the reasons why wave overtopping flow has more erosive power than overflow.

The hydraulic conditions, especially the amount of turbulence as well as the forces on the dike cover, are difficult to measure during overtopping experiments. One way to overcome this problem is to use a Computational Fluid Dynamic (CFD) model that provides information on all the hydraulic variables as function of time at all locations. This approach has found successful application in coastal engineering problems such as tsunami-induced scour around monopile foundations (Larsen et al., 2017), flow over coastal structures with porous media (Jensen et al., 2014) and the overtopping flow over flood defences with a complex configuration (Chen et al., 2021a; Van Bergeijk et al., 2020a), shallow foreshores (Suzuki et al., 2020), vertical walls (De Finis et al., 2020; Chen et al., 2021b; Jacobsen et al., 2018) or grass covers (Bomers et al., 2018; Van Bergeijk et al., 2020b). Additionally, the hydraulic boundary conditions and dike geometry can easily be adapted in a numerical model which makes is suitable to study the effect of these parameters on the overtopping load. Therefore, we follow a modelling approach to investigate the hydraulic load of overtopping waves on the dike cover.

The goal of this study is to investigate the hydraulic load generated by overtopping waves on the landward side of grass-covered flood defences. The hydraulic load is one of the main input variables in erosion models and both the magnitude and the location of the maximum hydraulic load are necessary to determine the location of failure along the dike profile. The location of maximum load depends on the loading mechanisms – shear forces at the landward toe or normal forces on the upper slope – as well as the main design parameters such as the hydraulic boundary conditions and the dike geometry. Practical load formulations are developed to include the effects of the main design parameters on the hydraulic load of grass-covered flood defences which can be used to describe the load in existing erosion models. The main contribution of this work is that we derived separate load formulations for the flow velocity, shear stress, normal stress and pressure in contrast to the existing formulas that are all related to the overtopping flow velocity.

The paper is organised as follows: Section 2 describes the numerical modelling approach and the derivation of the practical load formulations. In Section 3, the results are presented followed by the discussion and the conclusions in Sections 4 and 5 .

2. Method

In this study, we derive practical load formulations for the landward slope using the output of a numerical model that can be used in erosion models to predict where and when the grass cover will erode (Fig. 2). We use the numerical OpenFOAM® (OpenCFD Ltd., 2019) model setup used by Van Bergeijk et al. (2020b) to investigate the hydraulic load on the landward slope of grass-covered dikes This numerical model calculates the four hydraulic variables that are used to describe the load in existing erosion models – flow velocity, shear stress, normal stress and pressure – as function of time and location including the effect of turbulence. The model was previously validated for the flow velocity, layer thickness and pressure for both the magnitude as the variation in time (Van Bergeijk et al., 2020b). Additionally, the vertical flow structure was validated using the flow velocity near the bottom and in the top layer, which is used to calculate the shear stress within the model. However, flow separation at the crest line and impact on the upper slope was not modelled in previous studies due to the relative gentle slope of 1:3 and 1:5 (Van Bergeijk et al., 2020b; Bomers et al., 2018).

The normal forces expressed by the normal stress are validated in this study using the observed erosion during wave overtopping tests near Wijmeers in Belgium (Bakker and Mom, 2015). This grass-covered dike has a steep slope of 1:1.7 leading to erosion by wave impact around 1 m–2 m of the crest line. The normal stress during the experiment is modelled along the dike profile and compared to the observed erosion to validate the normal stress in the model, thereby assuming that the location of high normal stresses correlate with the location of erosion.

Next, practical formulations for the hydraulic variables are developed using the results of 54 model runs where the effect of three main design parameters on the load is determined: the overtopping volume, the slope steepness and the slope length (Section 3.2). These load formulations calculate the maximum expected hydraulic load and the location of the maximum load is determined as well.

The practical load formulations together with the detailed model output are used to calculate several erosion indices. These erosion indices depend on an erosion threshold and a hydraulic variable, either

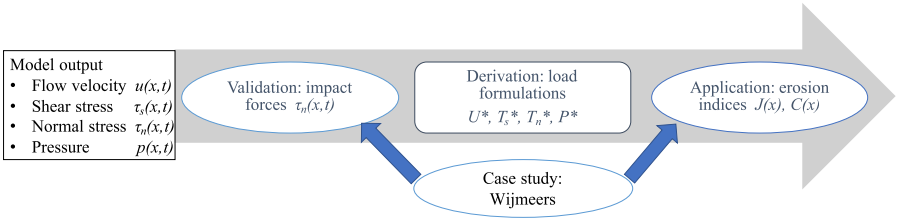

Fig. 2. Schematisation of the method. The model output is first used to validate the impact forces for the Wijmeers case. Next, the practical load formulations are derived followed by the calculations of the erosion indices for the Wijmeers case where we show how the derived load formulations and model output can be used.

the flow velocity, shear stress, normal stress or pressure, and indicate when and where erosion will occur. The amount of erosion itself is not calculated since erosion models use a different variable to express the amount of erosion, such as an erosion depth or a damage number (Van Bergeijk et al., 2021; Van der Meer et al., 2010), and the calculated erosion is therefore not comparable. The erosion indices provide a fair comparison of the erosive power in the different erosion models and can be transferred to an erosion depth using for example the erosion rate and duration. The erosion indices are calculated for the Wijmeers case study and show where the different indices predict erosion compared to the observed erosion during the experiment. This last step shows how the insights in the hydraulic load found in this study can be applied in erosion models for wave overtopping.

2.1. Case study: Wijmeers

Wave overtopping experiments on a dike with a steep slope (1 : 1.7) near Wijmeers resulted in failure of the grass cover on the upper slope (Van Damme et al., 2016; Ponsioen et al., 2019). The steep slope led to the flow separating from the crest line (Fig. 1c) and impacting on the upper slope where the high normal forces eroded the dike cover. The wave overtopping simulator (Van der Meer et al., 2007) was located 3 m from the crest line and the landward slope had a length of 6 m. This experiment is used in this study because the dike section at Wijmeers is the steepest slope tested using the wave overtopping simulator and therefore the flow separation at the end of the crest was clearly noted (Van Damme et al., 2016).

Five tests were performed with an increasing overtopping discharge q of 1, 5, 10, 25 and 50 l/s/m. No damage was observed during the first two tests ($q = 1$ and 5 l/s/m) and the observed damage during the test with the 10 l/s/m was related to a rabbit hole. The test with 50 l/s/m was stopped after 12 min because of the rapid erosion that followed on the damage during the 25 l/s/m test. Therefore, only the results of the test with 25 l/s/m are used in this study.

During this test, the grass cover was damaged between 1.3 m and 2.15 m from the crest line. The theoretical volume distribution consists of 858 overtopping waves with a maximum volume V of 1.662 m^3/m (Fig. 3). Small overtopping volumes ($V < 0.1$ m^3/m) were not simulated during the experiment due to technical limitations related to the opening and closing of the valves in the overtopping simulator resulting in 674 simulated waves during the experiment (Bakker and Mom, 2015). It is not possible to model all the overtopping waves during the test in the numerical model due to the high computational cost (Section 2.2). Therefore, the volume distribution was represented by seven volumes in the numerical model: 0.25, 0.5, 0.75, 1.0, 1.25, 1.5 and 1.662 m^3/m. These volumes are used to make a representative volume distribution (Fig. 3) similar to the method of Bomers et al. (2018) who showed that a schematised volume distribution is able to accurately simulate the erosion during an overtopping experiment.

2.2. Model set-up

Van Bergeijk et al. (2020b) developed a 2D-vertical hydrodynamic model for the overtopping flow over the crest and landward slope

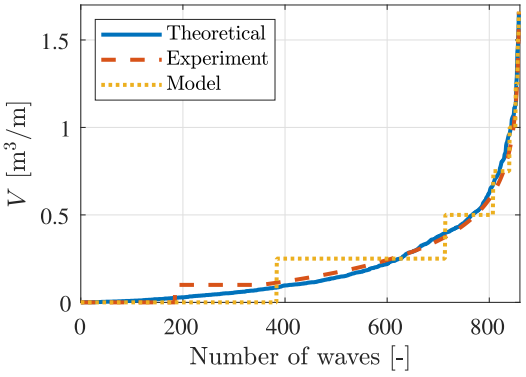

Fig. 3. The theoretical volume distribution for the Wijmeers test with $q = 25$ l/s/m together with all the volumes released during the experiment (red-dashed) and the schematised distribution in the model (yellow-dotted).

of grass-covered flood defences. This model is built using the open-source software OpenFOAM® v1806 and solves the Reynolds-Averaged Navier–Stokes equations. A k-ω SST turbulence model is used together with a Nikuradse roughness height of 8 mm for the grass cover as calibrated by Van Bergeijk et al. (2020b). The incoming wave consists of 80% of water and 20% of air similar to the measured air content of overtopping waves during field tests (Hoffmans, 2012). The boundary conditions are the time-dependent flow velocity u_0 and layer thickness h_0 on the dike crest generated using the overtopping volume (Van der Meer et al., 2010; Hughes and Shaw, 2011) (Fig. 4).

$$u_0(t) = 4.5\,V^{0.34}\left(1 - \frac{t}{T_0}\right) \quad \text{and} \quad h_0(t) = 0.133\,V^{0.5}\left(1 - \frac{t}{T_0}\right). \tag{1}$$

with the time t and overtopping duration T_0 (Van der Meer et al., 2010).

$$T_0 = 4.4V^{0.3} \tag{2}$$

Flow separation at the crest line was not observed during previous model simulations reported in Van Bergeijk et al. (2020b) due to the relative gentle slopes of the dike profiles. The grid was set to a grid size 1 cm x 1 cm (cross-dike Δx x vertical Δz) and the number of non-orthogonal correctors was increased to 3 to improve the simulation of flow separation at the transition from the crest to the slope (see Appendix B for a sensitivity analysis of the non-orthogonal correctors). The grid size is smaller than twice the roughness height, but the rough wall function in OpenFOAM is also applicable in these cases as shown by Larsen et al. (2017). Grid sizes of 0.8 cm and 1.2 cm showed similar results for the impact location and overtopping forces. Sensitivity analyses performed by Van Bergeijk et al. (2020b) showed that the modelled flow velocity and layer thickness were not sensitive to the roughness height and the grid size had no significant effect on the overtopping flow velocity.

The model domain consists of a crest width of 3 m, a slope with steepness $\cot(\varphi)$ and length L_s followed by a 2 m horizontal plane (Fig. 4). The output parameters presented in this study are the water

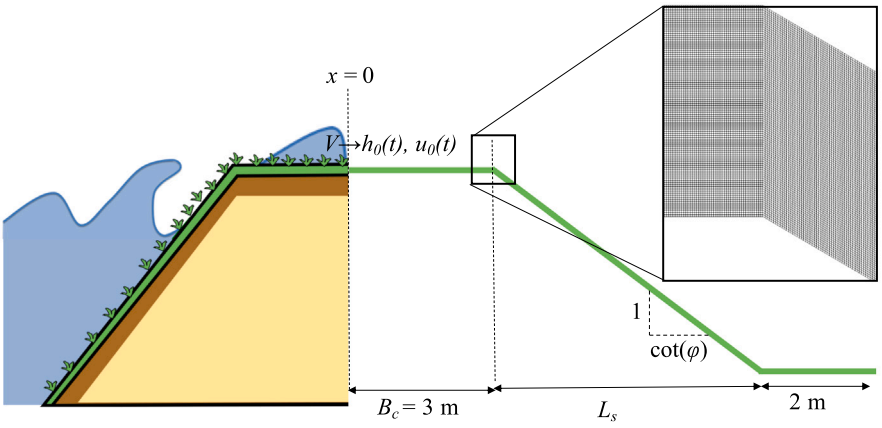

Fig. 4. The model domain starts at a cross-dike location $x = 0$ and includes a crest width B_c of 3 m, the landward slope and an additional 2 m after the landward toe with a close up of the model grid at the transition from the crest to the slope. Simulations are done with varying slope length L_s, slope steepness $\cot(\varphi)$ and overtopping volume V, which is translated to the layer thickness $h_0(t)$ and flow velocity $u_0(t)$ on the dike crest as function of time t.

fraction $\alpha_w(x,z,t)$ [-], flow velocity in the top layer of the overtopping wave $u(x,t)$ [m/s], the pressure on the dike surface $p(x,t)$ [Pa], the shear stress on the dike surface parallel to the dike surface $\tau_s(x,t)$ [N/m^2] and perpendicular to the dike surface $\tau_n(x,t)$ [N/m^2], hereafter named normal stress. The water fraction is 1 for water, 0 for air and between 0 and 1 for air–water mixtures. The flow velocity, pressure, shear stress and normal stress are multiplied by the water fraction to ensure that the model output only includes the water flow. Additionally, the shear stress and the normal stress are multiplied by the density of water to obtain the stress in N/m^2. The flow velocity is determined at every 0.5 m along the dike profile, while the other output variables are determined for every boundary cell along the dike profile with a spacing of 1 cm.

The computational time depends on the overtopping volume and the slope length, for example the simulation of one overtopping wave ($V = 1.5$ m^3/m) takes around 3 h for $L_s = 4$ m and increases to 9 h for $L_s = 20$ m using only one core on a standard computer with an Intel coreTM i7-9700 GHz(x12) processor. The small grid size is the main reason for the relatively large simulation time per wave and therefore it not possible to simulate an entire wave time series during a storm. For example, the 858 waves during the overtopping experiments in Wijmeers would take more than a month to simulate on a standard computer. While parallel computing can speed up the process, the model output per wave is around 30 GB which leads to an enormous amount of data for 858 waves. For these reasons, we use a schematised volume distribution to simulate the hydraulic load during the Wijmeers experiment similar to the method of Bomers et al. (2018).

2.3. Wave impact

2.3.1. Validation

The overtopping test with $q = 25$ l/s/m of the Wijmeers case is simulated to evaluate whether the model is capable of simulating the wave impact process. We follow a similar approach described in Ponsioen et al. (2019) where the erosive power during wave impact is expressed using the excess normal stress J_N. In the excess normal stress, the load is described by the normal stress integrated over the overtopping duration T_0 and the cover strength is described by the critical normal stress $\tau_{c,n}$ (Fig. 5). The excess normal stress indicates when and where damage is expected ($J_N > 0$) and is calculated as

$$J_N(x) = \sum_{n=1}^{N} \int_0^{T_0} \left(\tau_n(x,t) - \tau_{c,n}\right) \mathrm{d}t, \tag{3}$$

with the number of overtopping waves N.

A wide range of values for the critical normal stress can be found in literature where the grass cover strength depends on the grass quality, including vegetation type and coverage, and the underlying soil layer, often a mixture of clay and grass. Additionally, the erosion threshold described by the critical normal stress is model dependent since the magnitude of the hydraulic variables differs between models (Van Bergeijk et al., 2020b). To overcome this problem, the erosion threshold can be calibrated for a specific model using the load during overtopping tests where no erosion occurred (Van der Meer et al., 2010; Warmink et al., 2020; Ponsioen et al., 2019). The dike cover was not damaged by the load during these tests and therefore the maximum load during these tests is an indication of the load that the dike cover is able to withstand.

In the Wijmeers experiment, erosion of the grass cover was not observed during the test with $q = 5$ l/s/m with a maximum overtopping volume of 0.349 m^3/m. Therefore, the maximum normal stress with respect to time and space is calculated for this overtopping volume and used as the critical normal stress $\tau_{c,n}$ in this study (Table 1). The flow does not separate at the crest leading to no impact and a relatively small calibrated critical normal stress for this overtopping volume. Although the wave impact process is not captured in this calibrated value, this value is mainly used for comparison to other methods. Additionally, we determine the critical normal stress $\tau_{c,U}$ from the calibrated critical flow velocity U_c using

$$\tau_{c,U} = \frac{1}{2}\rho f U_c^2. \tag{4}$$

with the friction coefficient f is 0.01 for grass (SBW, 2012a). The calibrated critical velocity U_c corresponds to the maximum modelled flow velocity for $V = 0.349$ m^3/m similar to calibration method of $\tau_{c,n}$. The calibrated erosion thresholds are in the same order of magnitude as the literature values of Hoffmans (2012) and the calibrated values of Ponsioen et al. (2019). The differences between the values are the result of the erosion thresholds being model dependent. The values of Hoffmans (2012) give an indication for the erosion threshold of an average grass quality where the range indicate the uncertainty in the cover strength.

To validate the model for wave impact, the excess normal stress is calculated using the calibrated erosion thresholds $\tau_{c,n}$ and $\tau_{c,U}$. The location where the excess normal stress predicts erosion is compared to the observed damage during the overtopping test ($x = 1.3 - 2.15$ m) to see if the model is able to predict the location where the cover is damaged.

2.3.2. Conditions for wave impact

It is unclear under which conditions wave impact becomes the dominant failure mode compared to toe scour and therefore at which location the dike will fail exactly. Therefore, the conditions for wave

Table 1
The calibrated erosion thresholds for the flow velocity U_c, shear stress $\tau_{c,s}$, normal stress $\tau_{c,n}$, the pressure P_c and the stress $\tau_{c,U}$ calculated using Eq. (4) together with the thresholds of other studies.

Threshold	U_c [m/s]	$\tau_{c,s}$ [N/m^2]	$\tau_{c,n}$ [N/m^2]	$\tau_{c,U}$ [N/m^2]	P_c [kPa]
Calibrated	4.0	594	14.7	80	2.78
Hoffmans (2012)	3.0–5.0	50–125	50–125	50–125	5.3–7.5
Ponsioen et al. (2019)	3.5	–	–	–	4

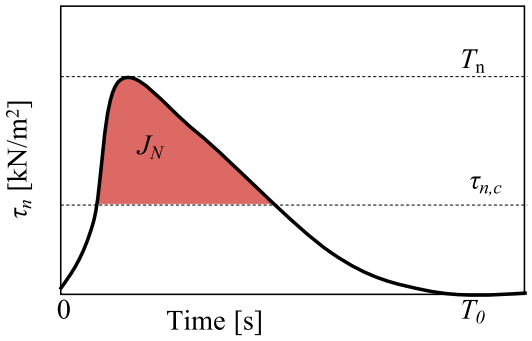

Fig. 5. The red area indicates the excess normal stress where the load is described by the normal stress τ_n as function of time t and the strength by the critical normal stress $\tau_{c,n}$. T_n is the maximum normal stress with respect to time and T_0 is the overtopping duration.

impact are determined as a first step of identifying the dominant failure mechanism for a range of flood defences. The conditions for wave impact provide a threshold of the overtopping volume per slope steepness that needs to be exceeded for wave impact to occur. Herein we differentiate between two threshold volumes: the volume where flow separation at the crest line is observed in the numerical simulations and the volume where the impact at the location of reattachment results in peaks in the normal stress and pressure on the upper slope that exceed the erosion threshold. Erosion due to wave impact is expected for volumes above the thresholds contrary to volumes below the thresholds. For overtopping volumes between the two thresholds, it remains uncertain if the normal stress is high enough to erode the grass cover.

These two threshold volumes are determined for 8 values of the slope steepness $\cot(\varphi)$: 1, 1.5, 1.7, 2, 2.2, 2.5, 2.7, 3.0. The overtopping volume in the model is increased in steps of 0.25 m^3/m between 0.25 and 5.5 m^3/m. The simulations with a slope steepness of 1.7 are representative for the Wijmeers case.

2.4. Practical load formulations

The overtopping volume, slope steepness, slope length and cover type are the four main design parameters that are used in design on the landward slope. The goal is to find a simple formulation for the maximum value of the four hydraulic variables as function of the volume, slope steepness and slope length for grass-covered flood defences. Additionally, the location where the variables have their maximal values is investigated in order to predict where the dike will most likely fail. The practical load formulations are developed following the approach of Capel (2015) and Chen et al. (2020) who both determined equations for the effect of roughness elements and berms on the waterside slope on the overtopping discharge.

As a first step, the hydraulic variables are made dimensionless to ensure that both sides of the load formulation have equal dimensions. The maximum flow velocity $u_0(t = 0)$ and the maximum layer thickness $h_0(t = 0)$ at the start of our model domain are used to arrive at dimensionless variables (Eq. (1)). The maximum dimensionless flow velocity U^*, maximum dimensionless shear stress T_s^*, the maximum dimensionless normal stress T_n^* and maximum dimensionless pressure P^* are defined as

$$U^* = \frac{\max(u(x,t))}{u_0} \tag{5}$$

$$T_s^* = \frac{\max(\tau_s(x,t))}{\rho u_0^2} \tag{6}$$

$$T_n^* = \frac{\max(\tau_n(x,t))}{\rho u_0^2} \tag{7}$$

$$P^* = \frac{\max(p(x,t))}{\rho g h_0} \tag{8}$$

where max denotes the maximum operator with respect to time and location, ρ is the density of water and g is the gravitational acceleration.

The effect of the overtopping volume (0.25 – 5.5 m^3/m), slope steepness (1:1–1:5) and slope length (4–20 m) on the hydraulic variables is determined using 54 model runs where one parameter was varied while keeping the other two parameters constant (Table A.4). This way, we study the effect of each parameter on the hydraulic variable separately. For each model run, the maximum dimensionless variables are calculated together with the location where these variables have their maximum value.

Next, a regression analysis is conducted to develop the practical load formulations for the dimensionless variables as function of the volume, slope steepness and slope length. For each variable, first the effect of the volume was determined, followed by the effect of slope steepness and finally the effect of slope length. The slope steepness is a dimensionless parameter; but the volume and slope length have dimensions m^2 and m, respectively. Although certain combinations of the volume and slope length can lead to a dimensionless parameter, these combinations are not preferred since an increase in load is expected for both increasing overtopping volume and increasing slope length. Therefore, the coefficients of the load formulation will have a dimension to ensure that the fit in total will be dimensionless.

Furthermore, wave impact occurred for only 27 runs which did not include sufficient information on the normal stress and impact location for larger overtopping volumes. Therefore 8 additional runs were necessary to determine the effect of the overtopping volume and slope steepness on the normal stress. Next to the load formulation of the dimensionless normal stress, these 35 runs are used to develop a formulation for the location of impact X where the normal stress is maximal.

The accuracy of the obtained load formulations for each variable are scored using the Nash–Sutcliffe efficiency factor NSE (Nash and Sutcliffe, 1970), which is calculated for the maximum dimensionless flow velocity as

$$NSE = 1 - \frac{\sum_{i=1}^{N}(U_{f,i}^* - U_{m,i}^*)^2}{\sum_{i=1}^{N}(U_{m,i}^* - \overline{U_m^*})^2} \tag{9}$$

with the number of runs N, the value during run i of the formulation $U_{f,i}^*$ or the model result $U_{m,i}^*$ and $\overline{U_m^*}$ the average of all model runs. The NSE is calculated for the formulations of the four hydraulic variables where a NSE of 1 indicates a perfect fit between the formulation and the model results while a NSE of 0 indicates that the formulation is as accurate as the mean of the model results.

2.5. Erosion indices

The erosive power of the overtopping wave can be expressed in several erosion indices based on the flow velocity, shear stress, normal stress and pressure. Following the definition of the excess normal stress J_N, the excess velocity J_U, excess shear stress J_S and excess pressure J_P are calculated using the integral over the overtopping period (Table 2).

The excess erosion indices require information of the variables over time, while most calculation methods only provide information on the maximum value with respect to time. The hydraulic variables reach

Table 2
The erosional indices for the four hydraulic variables. The excess indices are integrated over the duration of the individual waves and therefore include information of the load as function of time contrary to the cumulative indices that are based on the maximum load of an individual wave with respect to time.

Method	Variable	Formula
Excess	Flow velocity	$J_U(x) = \sum_{n=1}^{N} \int_0^{T_0} u(x,t) - U_c \, dt$
	Shear stress	$J_S(x) = \sum_{n=1}^{N} \int_0^{T_0} \tau_s(x,t) - \tau_{c,s} \, dt$
	Normal stress	$J_N(x) = \sum_{n=1}^{N} \int_0^{T_0} \tau_n(x,t) - \tau_{c,n} \, dt$
	Pressure	$J_P(x) = \sum_{n=1}^{N} \int_0^{T_0} p(x,t) - P_c \, dt$
Cumulative	Flow velocity	$C_U(x) = \sum_{n=1}^{N} U(x) - U_c$
	Shear stress	$C_S(x) = \sum_{n=1}^{N} T_s(x) - \tau_{c,s}$
	Normal stress	$C_N(x) = \sum_{n=1}^{N} T_n(x) - \tau_{c,n}$
	Pressure	$C_P(x) = \sum_{n=1}^{N} P(x) - P_c$

their maximum values at the wave front followed by a rapid decrease over time (Van Bergeijk et al., 2020b) and it is expected that this high load at the wave front causes the cover to erode, as illustrated with the maximum normal stress with respect to time T_n in Fig. 5. For example, the erosion models of Dean et al. (2010) and Hoffmans (2012) use the maximum flow velocity and replace the time integral by the overtopping duration as a multiplication factor. Van der Meer et al. (2010) concluded that erosion was caused by the impact of the maximum flow velocity during a short time period within the overtopping duration and therefore omitted the overtopping duration in the cumulative overload method. These types of models are a function of the maximum load with respect to time and are defined as cumulative loads, which still vary along the slope (Table 2).

The erosion by overtopping waves is time-dependent where we distinguish between two time scales: (1) the time scale of an individual wave expressed by the overtopping duration, and (2) the time scale of the storm expressed by number of overtopping waves. The effect of the time scale of an individual wave on the erosion is investigated in this study by comparing the excess indices and the cumulative indices, where this effect is only included in the excess indices.

The eight erosion indices in Table 2 are calculated for the Wijmeers test with $q = 25$ l/s/m using the schematised volume distribution (Fig. 3). The erosion thresholds indicated by U_c, $\tau_{s,c}$ and P_c are calibrated using the maximum flow velocity, shear stress and pressure with respect to time and space for an overtopping volume of 0.349 m^3/m similar to the critical normal stress (Table 1).

Additionally, the cumulative erosion indices are calculated using the practical load formulations to show how these formulations can be used in erosion models. This also shows the difference in erosion predictions using detailed information from the numerical model, such as the load as function of time along the dike profile, compared to a simple load formulation. The load of every overtopping wave can quickly be calculated using the formulations and therefore the cumulative indices are calculated based on every overtopping volume of the theoretical volume distribution instead of the schematised distribution (Fig. 3). The formulations for the flow velocity, shear stress and pressure only predict a maximum value and therefore the erosion indices are constant along the profile. The formulation for the normal stress is used in combination with the impact location and results in a cumulative normal stress along the dike slope.

3. Results

3.1. Wave impact

The model simulation for the Wijmeers case with $V = 1.662$ m^3/m shows that the overtopping flow separates from the dike profile at the crest line and reattaches on the landward slope (Fig. 6, see the supplementary material for a video). The impact of the flow on the upper slope leads to a high peak in the maximum normal stress $T_n(x)$ (Panel c) and maximum pressure $P(x)$ (Panel d). The peak in the normal stress ($x = 1.65 - 1.8$ m) is located slightly more landward compared to the peak in the pressure ($x = 1.65 - 2.1$ m). The flow separation at the crest line leads to a decrease in the flow velocity and shear stress on the upper slope ($x = 0 - 1.6$ m) followed by an increase back to their value at the end of crest at the location where the peaks in normal stress and pressure start ($x = 1.6$ m).

The normal stress is maximal on the upper slope where the flow reattaches to the dike profile. The pressure is shows both a peak at the upper slope and at the landward toe ($x = 6$ m) and therefore describes both the normal forces due to impact and the shear forces at the landward toe. The flow velocity and shear stress have their maximum values slightly landward of the toe ($x = 6.15$ m).

3.1.1. Validation

The observed damage during the overtopping test ($x = 1.3 - 2.15$ m) is compared to the location where the excess normal stress J_N predicts erosion to validate that the model is able to predict the location where the cover is damaged. The excess normal stress J_N is calculated for the Wijmeers test with $q = 25$ l/s/m by integration over the overtopping waves during the storm (Fig. 3) and shows three main peaks related to the impact location of the volumes 1 m^3/m at 0.9 m, 1.25 m^3/m at 1.2 m and 1.5 m^3/m at 1.7 m (Fig. 7). The maximum volume of 1.662 m^3/m does not lead to a clear peak since this volume only occurs once in the volume distribution and the peak partially overlaps with the peak of 1.5 m^3/m. The impact of 0.75 m^3/m is relatively small and only observed in a small peak around $x = 0.6$ m for $\tau_{c,n}$.

The excess normal stress calculated using the erosion threshold $\tau_{c,n}$ predicts most erosion between 0.8 and 1.7 m, which is closer to the crest compared to the erosion predicted using $\tau_{c,U}$ (1.3 – 2 m). The erosion threshold calculated from the critical velocity $\tau_{c,U}$ leads to no erosion at the landward toe (blue area) since the normal stress does not exceed the threshold in this case, while the smaller threshold $\tau_{c,n}$ results in erosion at the landward toe. Thus, the model is able to predict the location of observed cover damage where the use of the threshold $\tau_{c,U}$ leads to a better agreement between the excess normal stress and the observed damage location than the use of the threshold $\tau_{c,n}$.

3.1.2. Conditions

The overtopping volumes where the flow separates and impacts on the upper slope are determined for each slope steepness (Fig. 8). For overtopping volumes larger than this threshold, wave impact will occur and therefore the normal forces will likely dominate the shear forces leading to failure of the dike cover on the upper slope instead of the landward toe. The flow does not separate at the crest line for overtopping volumes smaller than these thresholds leading to small normal forces that are not able to erode the grass cover on the upper slope. The white area indicates the volumes where flow separation is observed in the model simulations but the impact does not lead to a noticeable peak in the normal stress. For these volumes, it is possible that impact occurs which might lead to erosion.

For gentle slopes with $\cot(\varphi) \geq 3$, the threshold volume for slope separation are larger than 5.0 m^3/m which has not been simulated during overtopping experiments yet and is extremely unlikely to occur. This high threshold explains why wave impact was not observed in previous model studies of the overtopping flow over the dike crest and landward slope (Bomers et al., 2018; Van Bergeijk et al., 2020b).

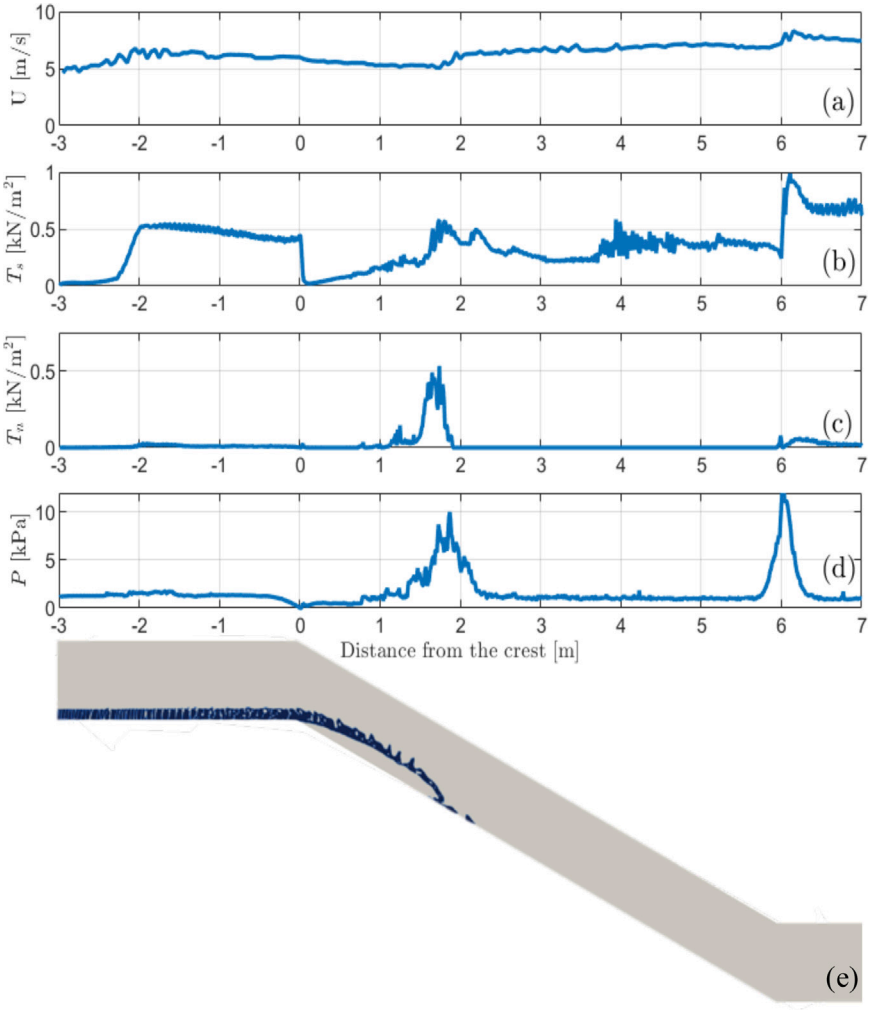

Fig. 6. Model results for an overtopping volume of 1.662 m^3/m at Wijmeers: (a) The maximum flow velocity $U(x)$, (b) The maximum shear stress $T_s(x)$, (c) The maximum normal stress $T_n(x)$, (d) The maximum pressure $P(x)$, (e) Snapshot of the water fraction α_w at 0.95 s.

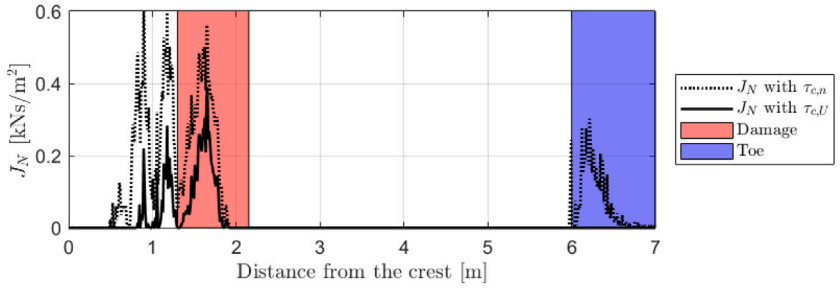

Fig. 7. The excess normal stress J_N for test q = 25 l/s/m at Wijmeers for the two erosion thresholds $\tau_{c,n}$ and $\tau_{c,U}$. (For interpretation of the references to colour in this figure legend, the reader is referred to the web version of this article.)

These models were applied to dikes with a gentle slope ($\cot(\varphi) \geq 3$) in combination with $V \leq 1.5$ m^3/m (Bomers et al., 2018) and $V \leq 4$ m^3/m (Van Bergeijk et al., 2020b), where no wave impact would have occurred according to these results.

3.2. Practical load formulations

The model runs show that the pressure, shear stress and flow velocity have their maximum values at the landward toe and therefore the practical load formulations for these three variables are developed for the load at the toe (Table 3, Fig. 9). The normal stress is maximal on the upper slope and therefore does not depend on the slope length, similar to the impact location. The dimensions of the coefficients in the formulations are 0.22 [m$^{-5/2}$], 11.9 [m$^{-6/5}$], 0.023 [m$^{-3/2}$], 0.15 [m$^{-2/5}$] and 6.21 [m$^{-4/5}$] to make the formulations dimensionless (Table 3). The results of the regression analysis are shown in Fig. A.11 in the appendix to denote the accuracy of the fits.

The modelled flow velocity is maximal at the end of the slope for almost all runs. For the other runs, the flow velocity is approximately constant along the slope resulting in a flow velocity at the toe close to the maximum flow velocity with a difference of less than 5%. This means that the flow velocity at the landward toe can be used to predict the maximum expected flow velocity.

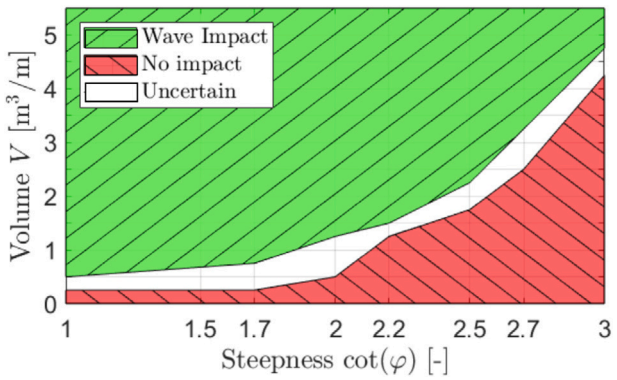

Fig. 8. The overtopping volumes V as function of the steepness of the landward slope for which significant wave impact forces were observed on the upper slope (green) or not (red). The wave impact process is uncertain for the white area in between. (For interpretation of the references to colour in this figure legend, the reader is referred to the web version of this article.)

Table 3
The practical load formulations of the hydraulic variables and the location of impact as function of the overtopping volume V, the slope steepness cot(φ) and the slope length L_s together with the Nash–Sutcliffe model efficiency factor NSE.

Variable	Formula	NSE
Flow velocity	$U^* = 0.22\,\frac{V\sqrt{L_s}}{\cot(\varphi)^2} + 1.16$	0.74
Pressure	$P^* = 11.9\,\frac{\sqrt{V}\,L_s^{1/5}}{\cot(\varphi)^2} + 0.95$	0.90
Shear stress	$T_s^* = 0.023\,\frac{\sqrt{V\,L_s}}{\cot(\varphi)^3} + 0.022$	0.77
Normal stress	$T_n^* = 0.15\,\frac{V^{1/5}}{1.5 + \cot(\varphi)} - 0.03$	0.41
Impact location	$X = 6.21\,\frac{V^{2/5}}{1.5 + \cot(\varphi)} - 0.75$	0.58

The practical load formulations have a NSE above 0.40 where values above 0.0 are in general viewed as an acceptable level of performance (Moriasi et al., 2007). This shows that the hydraulic load can be predicted well using the overtopping volume, slope steepness and slope length. The load shows for all five formulations an increase with the increasing overtopping volume, decreasing slope steepness and increasing slope length (Table 3). Larger overtopping volumes and steeper slopes result in a higher load as the result of a higher acceleration while a longer slope means that the wave can accelerate over a longer period. The slope steepness has the highest power in the formulations which suggests that the slope steepness has the largest effect on the hydraulic load. However, the presented fits represent the dimensionless variables that are made dimensionless using the flow velocity and layer thickness that both depend on the overtopping volume (Eq. (1)). The slope length has a smaller effect on the load because a balance between bottom friction and gravitational acceleration is reached on the slope where after the load does not increase anymore with increasing slope length (Van Bergeijk et al., 2019b).

3.2.1. Comparison with existing formulations

No measurements of the hydraulic load at the landward toe are available. Therefore, the new formulations for the maximum dimensionless flow velocity and the location of impact are compared to existing formulations. The maximum dimensionless flow velocity U^* is similar to the acceleration factor α_a introduced by Steendam et al. (2014) used to calculate the flow velocity on the slope U_s in the cumulative overload method (Van der Meer et al., 2010).

$$U_s = \alpha_a u_0 \tag{10}$$

The acceleration factor is empirically determined from wave overtopping tests on grass-covered dikes for steep and gentle slopes (Van Hoven and Van der Meer, 2017)

$$\begin{aligned} \alpha_a &= 1.4 \quad \text{for steep slopes with} \quad 2.3 < \cot(\varphi) \leq 4.5 \\ \alpha_a &= 1.2 \quad \text{for gentle slopes with} \quad \cot(\varphi) > 4.5. \end{aligned} \tag{11}$$

The variation in the maximum flow velocity along the crest and slope can be calculated using the analytical formulas of Van Bergeijk et al. (2019b). These analytical formulas are used to calculate the maximum flow velocity at the end of the slope. This maximum flow velocity U^*_{slope} is again made dimensionless by dividing by the flow velocity at the start of the crest

$$U^*_{slope} = \frac{\alpha}{\beta u_0} + \frac{\mu}{u_0}\exp\left(-3\,\alpha\,\beta^2\,L_s/\cos(\varphi)\right) \tag{12}$$

where the flow velocity at the end of the crest U_{crest} and the parameters μ, α and β are calculated as

$$\begin{aligned} U_{crest} &= \left(\frac{f\,B_c}{2h_0u_0} + \frac{1}{u_0}\right)^{-1} \\ \mu &= U_{crest} - \frac{\alpha}{\beta} \\ \alpha &= \sqrt[3]{g\sin\varphi} \\ \beta &= \sqrt[3]{f/2h_0u_0}. \end{aligned} \tag{13}$$

The analytical formulas are only applicable in cases where the friction factor is larger than the limiting friction factor f_{lim}

$$f_{lim} = \frac{g h_0 u_0 \sin(\varphi)}{4U^3_{crest}}. \tag{14}$$

Comparison of the practical load formulation of the flow velocity with the existing formulations for the flow velocity shows that the NSE of the flow velocity formulation (NSE = 0.56) is significantly better compared to the acceleration factor α_a of Steendam et al. (2014) (NSE = −0.05) and the analytical formula U^*_{slope} of Van Bergeijk et al. (2019b) (NSE = −0.61) (Fig. 9e). However, the acceleration factor and analytical formulas are not applicable for all model runs because the acceleration factor is undefined for steep slopes (cot(φ) < 2.3) and the limiting friction factor in the analytical model. Therefore, the NSE is based on a smaller number of points (N = 37 for α_a and N = 47 for U^*_{slope}) compared to the load formulation (N = 54).

The average modelled dimensionless flow velocity $\overline{U^*_{OpenFOAM}}$ is 1.44 which is close to α_a = 1.4 (Steendam et al., 2014) for slopes with 2.3 < cot(φ) < 4.5. However, the constant acceleration factor underestimates the acceleration – and thereby the maximum load – of 46% of the modelled waves. This is probably because the acceleration factor does not depend on the overtopping volume and has no direct relation to the slope steepness.

Additionally, the formulation for the impact location X is compared to the formulas of Ponsioen et al. (2019), where the location of impact of the wave front is calculated as

$$X = \frac{2\,u_0^2\,\tan(\varphi)}{g} \tag{15}$$

The modelled impact location varies between 0.5 and 3.4 m for all the model runs (Fig. 9d). The analytical formula of Ponsioen et al. (2019) predicts a larger impact location varying between 2 and 10.5 m, which is larger than the relatively small slope length of Wijmeers (L_s = 6 m).

3.3. Erosion indices

The excess erosion indices (left panels of Fig. 10) and cumulative erosion indices (right panels of Fig. 10) show a similar pattern along the profile which means that the time integration has a minor influence on the results. This justifies the use of solely the maximum of the hydraulic variable with respect to time which is more convenient to use and saves computational time.

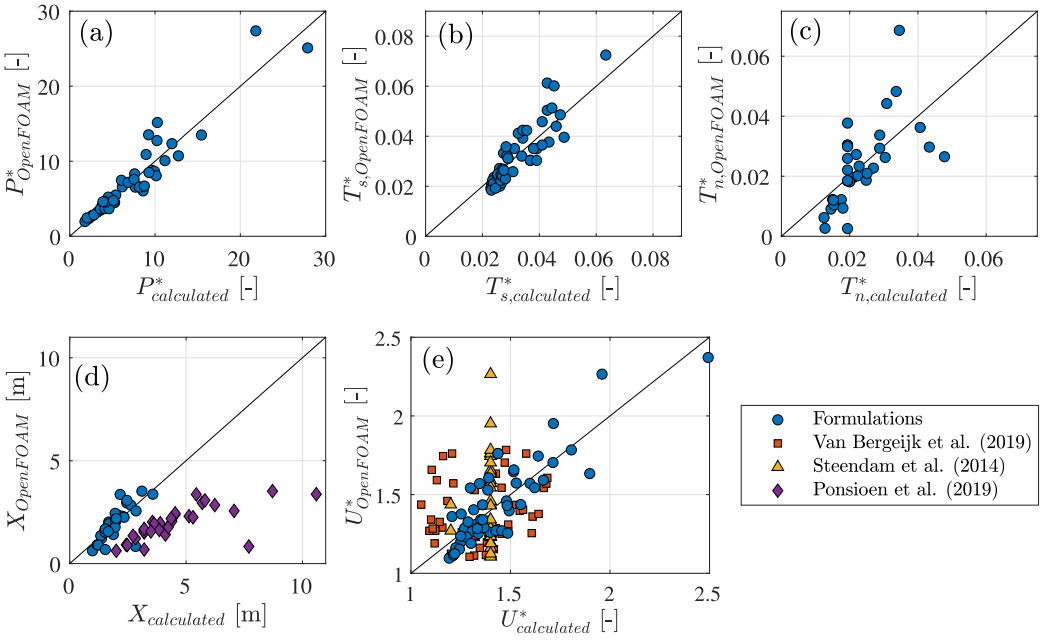

Fig. 9. The practical load formulations of the hydraulic variables as function of the overtopping volume, the slope steepness and the slope length (Table 3) compared to three existing formulations (Eqs. (11), (12) and (15)). (a) Dimensionless pressure $P*$, (b) Dimensionless shear stress T^*_s. (c) Dimensionless normal stress T^*_n, (d) The location of impact X, (e) Dimensionless flow velocity U^*.

The flow velocity indices predict erosion along the entire landward slope with most erosion after the landward toe. The shear stress and pressure indices predict solely dike cover erosion at the landward toe. The calibrated critical shear stress is relatively large compared to the literature value (Table 1) and is therefore only exceeded at the landward toe where the shear stress is maximal (Fig. 6b). Wave impact resulted in high peaks in the pressure on the upper slope (Fig. 6d), but the erosion indices for the pressure are completely dominated by the peak pressure at the landward toe.

The cumulative erosion indices using the load formulations (dashed, Fig. 10) are of similar magnitude compared to the erosion indices calculated with the model output. The difference in magnitude might be caused by the difference in volume distribution where the theoretical volume distribution with 858 overtopping volumes is used for the load formulations compared to the schematised distribution for the model output. This theoretical volume distribution also results in a continuous peak in the cumulative normal stress C_N compared to the separate peaks in the model output. The load formulation for the normal stress is able to predict the location of most erosion during the test and the order of magnitude is similar to the numerical model results.

4. Discussion

The model is able to predict the overtopping flow for both steep (1:1) and gentle (1:5) slopes with varying slope length. The volumes simulated in our model range between 0.25 m^3/m and 5.5 m^3/m. For smaller volumes, the water depths are too small to observe in the numerical model and the field, for example the layer thickness of V = 0.2 m^3/m was too small to be measured during wave overtopping tests with individual waves (SBW, 2012b). This has no significant impact on the erosion predictions, since the loads of these overtopping volumes are generally smaller than the erosion threshold and therefore have a negligible contribution to the erosion. The numerical model simulates the overtopping flow of long-crested waves perpendicular to the dike similar to the overtopping flows in flume experiment and field tests with the wave overtopping simulator. Therefore, the results of this study are only applicable to long-crest perpendicular waves and the model needs to be extended to a 3D model to study the effect of short-crested and oblique waves. 3D overtopping experiments with oblique waves have been performed for hard structures and the flow over the waterside slope (van Gent, 2021; EurOtop, 2018; Oosterlo et al., 2021). However, these types of experiments have not been performed for overtopping flow over crest and landward slope and therefore a 3D model cannot be validated at the moment.

The numerical model is validated for wave impact based on one overtopping field experiment with a steep slope. Most overtopping field tests are performed on dikes with gentler slopes where wave impact is not the dominant failure mechanism. The measured flow velocities, layer thicknesses and pressures of two experiments were previously used to validate the numerical model for gentler slopes without wave impact (Van Bergeijk et al., 2020b). Flow separation and wave impact can still occur on these slopes for larger overtopping volumes. Therefore, overtopping tests with larger volumes on gentle slopes can help to provide measurements of the wave impact process and to further validate both analytical and numerical models. The use of a 2DV model means that the inflow of air from the sides and the escape of air to the sides is not included in the model. The same limitation holds for overtopping tests where the inflow and escape of air is limited due the use of the hardwood boards.

In this study, the overtopping flow over a grass-covered dike is simulated using a Nikuradse roughness height of 8 mm in the turbulence model. Therefore, the practical load formulations are only applicable for grass-covered flood defences. Van Bergeijk et al. (2020b) showed that the roughness height only has a minor effect on the overtopping flow and therefore the calibrated roughness height is applicable for similar grass covers in Western Europe. The maximum hydraulic variables are expected to depend on the cover type and the formulations could be extended to other cover types using the roughness height or another type of roughness factor such as the Darcy–Weisbach friction factor (Scheres et al., 2020). It is also possible to extend the equations to include the effect of a berm or roughness elements as shown by Chen et al. (2021a) for the overtopping discharge.

The practical load formulations are valid in the modelled range (Table A.4: V = 0.25–5.5 m^3/m, $\cot(\varphi)$ = 1–5 and L_s = 4–20 m).

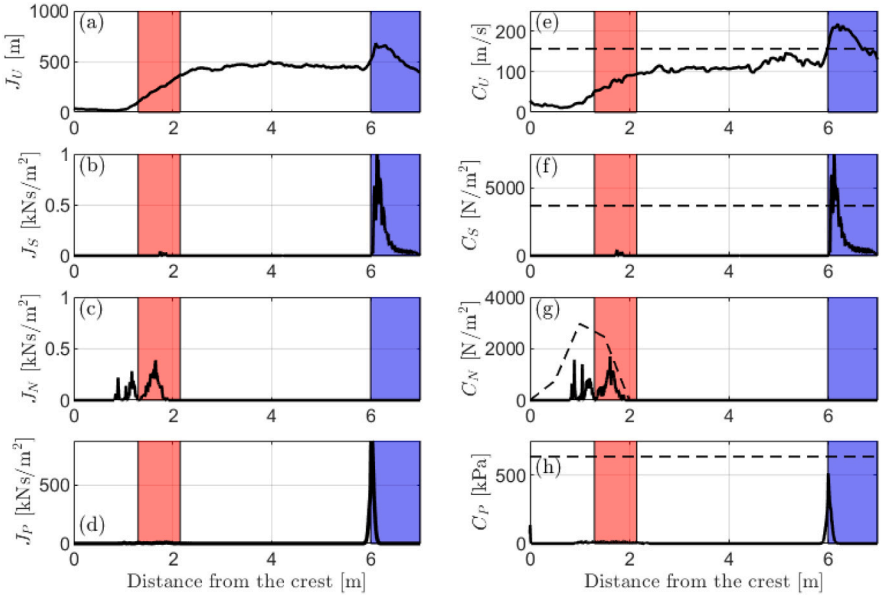

Fig. 10. The erosion indices for the Wijmeers experiment using the model output (solid) and load equations (dashed) with the location where cover eroded (red box) and the landward toe (blue box): (a) Excess velocity J_U. (b) Excess shear stress J_S. (c) Excess normal stress J_N. (d) Excess pressure J_P. (e) Cumulative flow velocity C_U. (f) Cumulative shear stress C_S. (g) Cumulative normal stress C_N. (h) Cumulative pressure C_P. (For interpretation of the references to colour in this figure legend, the reader is referred to the web version of this article.)

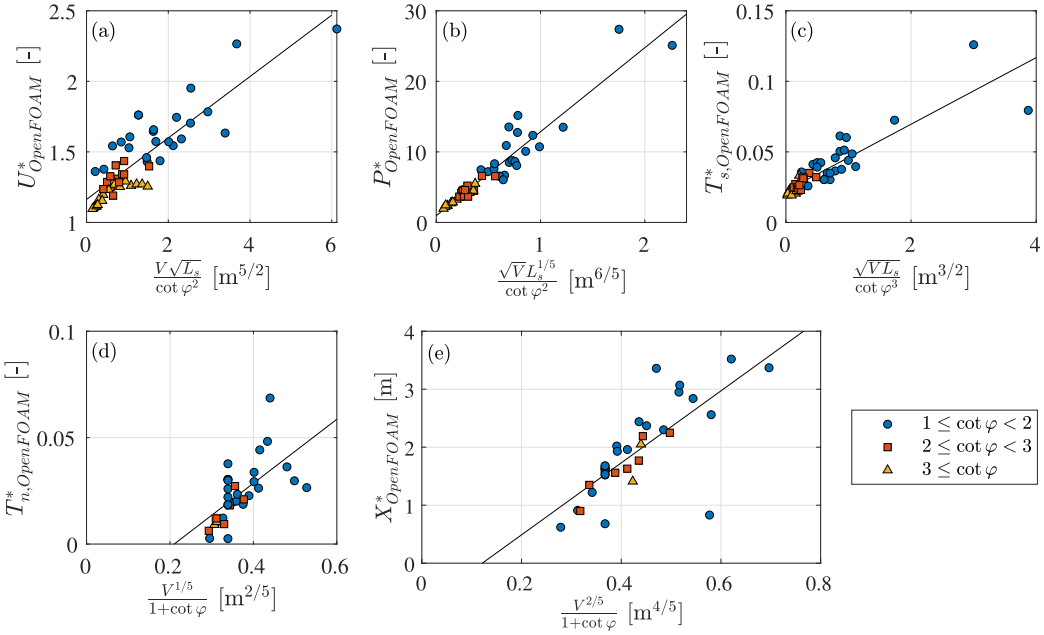

Fig. A.11. The fits resulting from the regression analysis used to develop the practical load equations: (a) Dimensionless flow velocity U^*, (b) Dimensionless pressure $P*$, (c) Dimensionless shear stress T_s^*. (d) Dimensionless normal stress T_n^*, (e) The location of impact X.

The load formulations for the normal stress and impact location are only valid under the conditions of wave impact which is represented by the green area in Fig. 8. This is also indicated by the negative offset of −0.03 and −0.75 in the load formulations (Table 3) that shows the minimum combination of volume and slope steepness required for wave impact to occur. The positive offset in the formulations for the flow velocity, pressure and shear stress are related to the landward toe where the slope change results in an additional load. This means that the load is larger at the landward toe compared to the crest for all model runs indicated by a positive offset. The additional load at the landward toe is simulated by a multiplication factor for the flow velocity in erosion models. The load factor in the cumulative overload method ranges between 1 and 2 and varies between 1.05 and 1.21 for the slope change at the landward toe (Hoffmans et al., 2018). The turbulence parameter in the analytical grass-erosion model increases from 2.0 on the slope to 2.75 at the landward toe (Warmink et al., 2020; Van Bergeijk et al., 2021), which corresponds to a multiplication factor of 1.375. Thus, the offset of 1.25 in the load formulation of the flow velocity is in line

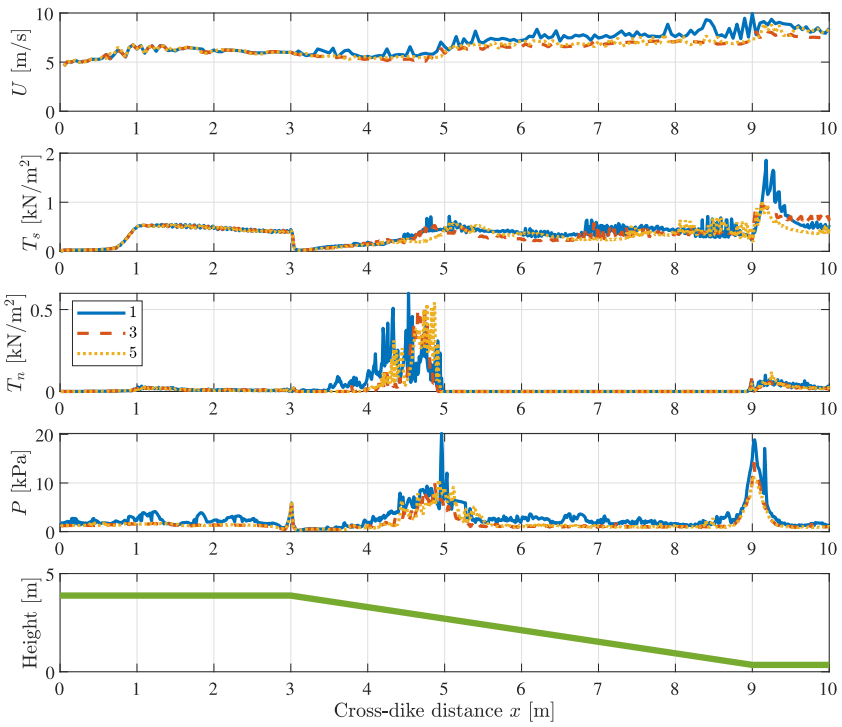

Fig. B.12. Results of the sensitivity analysis of the non-orthogonal correctors for an overtopping volume of 1.662 m^3/m at Wijmeers: (a) The maximum flow velocity $U(x)$, (b) The maximum shear stress $T_s(x)$, (c) The maximum normal stress $T_n(x)$, (d) The maximum pressure $P(x)$, (e) The dike profile.

with current multiplication factors for the load at the landward toe. No measurements of the flow velocity at the landward toe are available to validate the derived practical load formulation. In the future, we recommend performing hydraulic measurements at the landward toe for further validation of the practical load formulations.

The load formulations calculate the maximum expected load of an individual overtopping wave and are not directly applicable for wave parameters such as the significant wave height. The significant wave height in combination with other parameters such as the storm duration and outer slope geometry can be used to derive a volume distribution of overtopping waves (EurOtop, 2018; Van Bergeijk et al., 2019a). This volume distribution can be used similarly to the cumulative indices in the Wijmeers case study where the load during the storm is computed by a summation of the load by the individual waves. The numerical model can be extended to simulate the wave propagation and wave run-up on the waterside slope so that the load formulations can be related to wave parameters. However, this is computationally expensive and can only be done for short wave series of around 10 min (Chen et al., 2021a) and not for an entire storm duration of 6–12 h.

The model output and the derived practical load equations were used to calculate 8 erosion indices. A comparison of the excess and cumulative indices showed a similar pattern along the dike profile. The integration over time for the excess indices does not provide additional information while it is computationally more demanding. The high load at the wave front during a short duration is the main driving force of dike cover erosion, similar to the conclusion reached by Van der Meer et al. (2010) for the flow velocity. Therefore, we advise to use a cumulative index (Dean et al., 2010; Van der Meer et al., 2010; Hoffmans, 2012; Van Bergeijk et al., 2021) instead of an excess index (Aguilar-López et al., 2018; Ponsioen et al., 2019).

It is important to realise that one individual wave does not lead to damage of the grass cover and multiple overtopping waves during a longer time period are necessary to erode the grass cover. Although the erosion indices show that the erosion is not affect by the time scale of an individual wave, the time scale of the storm determines the number of overtopping waves and therefore has a major effect on the amount of erosion. Additionally, the erosion process by overtopping waves depends on time scales smaller than the storm duration when follow-up mechanisms such as head-cut erosion or the interaction with other failure mechanisms are considered (Van Bergeijk et al., 2021).

The flow velocity, shear stress and pressure indices predict most erosion at the landward toe related to the shearing forces. The flow velocity predicts erosion along the entire slope with most erosion after the landward toe, while the pressure and shear stress only predict erosion at the landward toe. In case of a constant grass cover strength along the profile, the dike will fail at the toe due to the shearing mechanism. However, the dike can also fail on the slope due to shearing at a weak spot where the erosion threshold is lower. This type of failure can only be described by the flow velocity since the pressure and shear stress indices are negligibly small on the slope and do not predict any erosion on the slope. The small shear stress on the slope is the result of the high calibrated erosion threshold $\tau_{s,n}$ (Table 1) that is 3 times larger compared to the value of Hoffmans (2012). This high shear stress at the landward toe also dominates the erosion indices of the shear stress. For erosion by shear loading, the maximum flow velocity at the landward toe can be calculated with the new practical formulation. However, analytical models or numerical models are necessary to calculate the flow velocity along the dike profile to describe grass failure in case of weak spots (Van Bergeijk et al., 2021; Hoffmans, 2012).

The normal stress is the only variable that proved able to predict erosion as the result of normal forces and therefore an erosion index based on the normal stress is required to describe the erosion in case of wave impact. The normal stress is small when wave impact does not occur and therefore the calibrated critical normal stress $\tau_{c,n}$ is not representative for the cover strength (see Section 2.3.1 for a description of the calibration process). For this reason, we propose to determine the erosion threshold for the normal stress $\tau_{c,U}$ from calibration of the critical flow velocity. This erosion threshold was able to predict the

location of observed erosion during the overtopping test at Wijmeers more accurately compared to the erosion threshold $\tau_{c,n}$. The excess normal stress showed several peaks related to the modelled volumes, where we used seven volumes to schematise the volume distribution. The excess normal stress becomes a continuous peak in case all volumes are modelled similar to cumulative normal stress calculated using the practical load formulations (Fig. 10g).

The eight erosion indices were not able to predict erosion by both loading mechanisms simultaneously. The conditions for wave impact can be used to provide a first estimate if wave impact will occur, otherwise the dike will fail due to the shear forces. In case of wave impact, an erosion model based on normal loading such as the analytical model of Ponsioen et al. (2019) is required while in cases without wave impact a shear-based model such as the analytical grass-erosion model (Van Bergeijk et al., 2021) or the cumulative overload method (Van der Meer et al., 2010) is preferred. Further research is necessary to determine when the normal loading will dominate over the shear loading in case of wave impact. This can mainly be obtained from erosion experiments such as the experiment at Wijmeers. Additionally, this type of information can be used to develop an erosion index that is able to predict both loading mechanisms simultaneously. For example, Ponsioen et al. (2019) suggested to use the total stress for dike cover erosion so both loading mechanisms are included. Our results show that the shear stress indices are larger than the normal stress indices for both the excess as the cumulative indices (Fig. 10). Therefore, the total stress would predict dike cover erosion at the landward toe due to the higher shear stress contrary to the observed erosion on the upper slope during the test. A possible solution could be to weight the normal and shear stress in an erosion formulation. Another option would be to use the pressure which shows both a peak on the upper slope as the result of normal loading and a peak at the landward toe due to shear loading. A different erosion threshold for the normal forces and shear forces could be used in the erosion formulation for the pressure to predict both mechanisms. With such adaptations, the erosion index for the total stress or pressure might be able to describe both loading mechanisms.

The erosion indices were only presented for one value of the threshold in this paper, since the magnitude of the threshold had no major effect on the erosion pattern along the slope. An increase in the threshold leads to no erosion on the upper slope for the flow velocity indices and no erosion at the landward toe for the normal stress indices (Fig. 7). A decrease in the threshold results in some erosion predicted by the shear stress on the crest and lower slope, similar to the flow velocity. For all threshold values, the location where most erosion is predicted remains the same, but the magnitude increases when the threshold decreases. This is expected since the threshold depends on the cover strength: a lower threshold indicates a lower cover strength leading to more erosion.

5. Conclusions

The wave overtopping load on the slope of a grass-covered dike is investigated using a numerical model in the open-source software OpenFOAM®. The model is able to simulate the details of the wave impact process where the flow separates from the dike profile at the crest line and reattaches on the landward slope. The model results show that this impact results in a high peak in the normal stress and pressure. The impact was validated using the observed erosion during overtopping tests on a grass-covered dike in Belgium. Additionally, the conditions for wave impact are determined in this study. This is an important finding to understand and predict when the wave impacts and thereby normal loading will occur, or shear loading is the only loading mechanism for a flood defence.

Practical load formulations for the maximum flow velocity, maximum shear stress, maximum normal stress, maximum pressure and impact location are determined from a regression analysis of the numerical results. The flow velocity, shear stress and pressure are maximal at the landward toe while the normal stress is maximal at the location of impact. The formulation for the maximum flow velocity showed to predict the flow velocity on grass-covered flood defences more accurately compared to existing formulations. The formulations are based on simulations with overtopping volumes between 0.25 m^3/m and 5.5 m^3/m, slopes with a steepness between 1:1 and 1:5 and slopes lengths varying from 4 m to 20 m. The formulations are only applicable to grass-covered flood defences within this range and need to be developed further for other cover types.

The practical load formulations provide a basis for erosion models to calculate dike cover failure by overtopping waves. The new formulations and the model output were used to calculate eight erosive indices that predict when and where the grass cover will erode. The excess indices and cumulative indices show the same variation along the dike profile which means that the additional information of the hydraulic variables over time required for the excess indices showed no added value for erosion models. The flow velocity has the most potential to describe the shear loading as the result of high flow velocities and turbulence and the normal stress is the only erosion index able to describe the normal loading as the result of wave impact.

The hydraulic variables were not able to predict both loading mechanisms simultaneously, nevertheless the erosion indexes of the pressure and total stress show potential for this end. Additional erosion tests with overtopping waves are necessary to further investigate when the erosion by wave impact on the upper slope will dominate over erosion by shear forces, since this depends not only on the magnitude of the load but also on the resistance of the grass cover for both loading mechanisms.

List of symbols

B_c	crest width	[m]
$C_N(x)$	cumulative normal stress	[N/m^2]
f	friction factor	[-]
h_0	layer thickness on the crest	[m]
$J_N(x)$	excess normal stress	[N s/m^2]
L_s	horizontal length of the landward slope	[m]
$p(x,t)$	pressure	[Pa]
$P(x)$	maximum pressure with respect to time	[Pa]
P^*	dimensionless pressure	[-]
t	time	[s]
$T_n(x)$	maximum normal stress with respect to time	[N/m^2]
T_n^*	dimensionless normal stress	[-]
$T_s(x)$	maximum shear stress with respect to time	[N/m^2]
T_s^*	dimensionless shear stress	[-]
$u(x,t)$	overtopping flow velocity	[m/s]
u_0	flow velocity on the crest	[m/s]
$U(x)$	maximum overtopping flow velocity with respect to time	[m/s]
U^*	dimensionless flow velocity	[-]
V	overtopping volume	[m^3/m]
x	cross-dike coordinate	[m]
X_{impact}	horizontal distance from the crest line where the wave impacts	[m]
z	vertical coordinate	[m]
α_a	acceleration factor	[-]
φ	angle of the landward slope	[°]
$\tau_n(x,t)$	normal stress perpendicular to the dike profile	[N/m^2]
$\tau_s(x,t)$	shear stress parallel to the dike profile	[N/m^2]

Table A.4
Settings of the 54 model runs to determine the effect of volume, slope steepness and slope length on the hydraulic variables and the 8 additional model runs for the normal stress τ_n and impact location X.

Parameter	Constant	Runs
Volume V	$L_s = 6$ m; $\cot(\varphi) = 1.7$	0.25–2.0 m^3/m, $\Delta = 0.25$ m^3/m
	$L_s = 6$ m; $\cot(\varphi) = 1.7$	2.5–4.0 m^3/m, $\Delta = 0.5$ m^3/m
	$L_s = 6$ m; $\cot(\varphi) = 3$	1.0–5.5 m^3/m, $\Delta = 0.5$ m^3/m
Steepness $\cot(\varphi)$	$L_s = 6$ m; $V = 1.5$ m^3/m	1, 1.5, 1.7, 2, 2.2, 2.5, 2.7 + 3–5, $\Delta = 1$
	$L_s = 6$ m; $V = 2.5$ m^3/m	1–5, $\Delta = 1$
Slope length L_s	$V = 1.5$ m^3/m, $\cot(\varphi) = 1.7$	4, 6, 8, 10, 12, 15, 18, 20 m
	$V = 1.5$ m^3/m, $\cot(\varphi) = 2.7$	4, 6, 8, 10, 12, 15, 18, 20 m
Runs for τ_n, X	$L_s = 6$ m, $V = 3$ m^3/m	$\cot(\varphi) = 1$, 1.5, 2 and 2.5
	$L_s = 6$ m, $V = 4$ m^3/m	$\cot(\varphi) = 1$, 1.5, 2 and 2.5

CRediT authorship contribution statement

Vera M. van Bergeijk: Conceptualisation, Methodology, Software, Validation, Writing – original draft, Writing – review & editing, Visualisation. **Jord J. Warmink:** Conceptualisation, Methodology, Writing – review & editing, Supervision, Project administration, Funding acquisition. **Suzanne J.M.H. Hulscher:** Conceptualisation, Writing – review & editing, Supervision, Project administration, Funding acquisition.

Declaration of competing interest

The authors declare that they have no known competing financial interests or personal relationships that could have appeared to influence the work reported in this paper.

Acknowledgements

This work is part of the research programme All-Risk, with project number P15-21, which is (partly) financed by the Netherlands Organisation for Scientific Research (NWO). The authors would like to thank Myron van Damme (Rijkswaterstaat) for providing the data of the Wijmeers experiments as well as some movies of the wave overtopping flow at the crest line. We would also like to thank Marcel Bottema (Rijkswaterstaat) for his feedback.

Appendix A. Regression analysis

Appendix B. Sensitivity analysis non-orthogonal correctors

A sensitivity analysis of the number of non-orthogonal correctors was performed where an overtopping volume of 1.662 m^3/m for the Wijmeers case was simulated with 1, 3 and 5 non-orthogonal correctors (Fig. B.12). The non-orthogonal correctors are required to accurately simulate the flow at the transition from the crest to the slope. The modelled hydraulic variables show therefore similar behaviour on the crest, but the number of non-orthogonal correctors affects the hydraulic variables on the landward slope.

The use of only 1 corrector results in a higher flow velocity on the slope, a higher shear stress after the landward toe and the location of impact is closer to the crest line as observed in the peaks in the normal stress compared to the use of 3 or 5 correctors. The modelled pressure using corrector 1 is slightly higher compared to 3 or 5 correctors but shows overall the same behaviour along the slope. The increase from 3 to 5 correctors does not significantly affect the modelled flow, which means that 3 non-orthogonal correctors are sufficient to simulate the overtopping flow including flow separation at the crest line.

Appendix C. Supplementary data

Supplementary material related to this article can be found online at https://doi.org/10.1016/j.coastaleng.2021.104047.

References

Aguilar-López, J.P., Warmink, J.J., Bomers, A., Schielen, R.M.J.J., Hulscher, S.J.M.H., 2018. Failure of grass covered flood defences with roads on top due to wave overtopping: A probabilistic assessment method. J. Mar. Sci. Eng. 6 (3), 1–28. http://dx.doi.org/10.3390/jmse6030074, URL: http://www.mdpi.com/2077-1312/6/3/74.

Bakker, J., Mom, R., 2015. Factual Report: Overslagproef Wijmeers 2 (in Dutch). Technical Report, Infram, Maarn, The Netherlands.

Blöschl, G., Hall, J., Viglione, A., Perdigão, R.A., Parajka, J., Merz, B., Lun, D., Arheimer, B., Aronica, G.T., Bilibashi, A., Boháč, M., Bonacci, O., Borga, M., Čanjevac, I., Castellarin, A., Chirico, G.B., Claps, P., Frolova, N., Ganora, D., Gorbachova, L., Gül, A., Hannaford, J., Harrigan, S., Kireeva, M., Kiss, A., Kjeldsen, T.R., Kohnová, S., Koskela, J.J., Ledvinka, O., Macdonald, N., Mavrova-Guirguinova, M., Mediero, L., Merz, R., Molnar, P., Montanari, A., Murphy, C., Osuch, M., Ovcharuk, V., Radevski, I., Salinas, J.L., Sauquet, E., Šraj, M., Szolgay, J., Volpi, E., Wilson, D., Zaimi, K., Živković, N., 2019. Changing climate both increases and decreases European river floods. Nature 573 (7772), 108–111. http://dx.doi.org/10.1038/s41586-019-1495-6.

Bomers, A., Aguilar-López, J.P., Warmink, J.J., Hulscher, S.J.M.H., 2018. Modelling effects of an asphalt road at a dike crest on dike cover erosion onset during wave overtopping. Nat. Hazards 93 (1), 1–30. http://dx.doi.org/10.1007/s11069-018-3287-y.

Bottema, M., Gunn, N., Van Haastrecht, B., Vonk, B., Van Hemert, H., 2021. Managing drought effects on levees in The Netherlands and England. In: FLOODrisk 2020 – 4th European Conference on Flood Risk Management Scale. Budapest University of Technology & Economics (BME), http://dx.doi.org/10.3311/FLOODRisk2020.8.1.

Capel, A., 2015. Wave run-up and overtopping reduction by block revetments with enhanced roughness. Coast. Eng. 104, 76–92. http://dx.doi.org/10.1016/j.coastaleng.2015.06.007.

Chen, W., van Gent, M.R.A., Warmink, J.J., Hulscher, S.J.M.H., 2020. The influence of a berm and roughness on the wave overtopping at dikes. Coast. Eng. 156 (September 2019), 103613. http://dx.doi.org/10.1016/j.coastaleng.2019.103613.

Chen, W., Warmink, J.J., Van Gent, M.R.A., Hulscher, S.J.M.H., 2021a. Numerical modelling of wave overtopping at dikes using OpenFOAM®. Coast. Eng. 166, http://dx.doi.org/10.1016/j.coastaleng.2021.103890, URL: https://doi.org/10.1016/j.scitotenv.2019.135907.

Chen, H., Yuan, J., Cao, D., Liu, P.L.F., 2021b. Wave overtopping flow striking a human body on the crest of an impermeable sloped seawall. Part II: Numerical modelling. Coast. Eng. 168, 103892. http://dx.doi.org/10.1016/J.COASTALENG.2021.103892.

De Finis, S., Romano, A., Bellotti, G., 2020. Numerical and laboratory analysis of post-overtopping wave impacts on a storm wall for a dike-promenade structure. Coast. Eng. 155, 103598. http://dx.doi.org/10.1016/J.COASTALENG.2019.103598.

Dean, R.G., Rosati, J.D., Walton, T.L., Edge, B.L., 2010. Erosional equivalences of levees: Steady and intermittent wave overtopping. Ocean Eng. 37 (1), 104–113. http://dx.doi.org/10.1016/j.oceaneng.2009.07.016.

EurOtop, 2018. Manual on Wave Overtopping of Sea Defences and Related Structures. An Overtopping Manual Largely Based on European Research, but for Worldwide Application. www.overtopping-manual.com. Technical Report, Authors: Van der Meer, J.W. Allsop, N.W.H. Bruce, T. De Rouck, J. Kortenhaus, A. Pullen, T. Schüttrumpf, H. Troch, P. Zanuttigh, B., URL: www.overtopping-manual.com.

Hoffmans, G.J.C.M., 2012. The Influence of Turbulence on Soil Erosion. Eburon Uitgeverij BV.

Hoffmans, G., Van Hoven, A., Steendam, G., van der Meer, J., 2018. Summary of research work about erodibility of grass revetments on dikes. In: Proc. Protections 2018 3th International Conference Against Overtopping, Grange-over-Sands, UK.

Hughes, S.A., 2011. Adaptation of the Levee Erosional Equivalence Method for the Hurricane Storm Damage Risk Reduction System (HSDRRS). Technical Report, U.S. Army Corps of Engineers, pp. 1–142.

Hughes, S.A., Shaw, J.M., 2011. Continuity of instantaneous wave overtopping discharge with application to stream power concepts. J. Waterw. Port Coast. Ocean Eng. 137 (1), 12–25. http://dx.doi.org/10.1061/(ASCE)WW.1943-5460.0000057.

Jacobsen, N.G., van Gent, M.R.A., Capel, A., Borsboom, M., 2018. Numerical prediction of integrated wave loads on crest walls on top of rubble mound structures. Coast. Eng. 142, 110–124. http://dx.doi.org/10.1016/J.COASTALENG.2018.10.004.

Jensen, B., Jacobsen, N.G., Christensen, E.D., 2014. Investigations on the porous media equations and resistance coefficients for coastal structures. Coast. Eng. 84, 56–72. http://dx.doi.org/10.1016/j.coastaleng.2013.11.004.

Larsen, B.E., Fuhrman, D.R., Baykal, C., Sumer, B.M., 2017. Tsunami-induced scour around monopile foundations. Coast. Eng. 129 (July), 36–49. http://dx.doi.org/10.1016/j.coastaleng.2017.08.002.

Moriasi, D.N., Arnold, J.G., Van Liew, M.W., Bingner, R.L., Harmel, R.D., Veith, T.L., 2007. Model evaluation guidelines for systematic quantification of accuracy in watershed simulations. Trans. ASABE 50 (3), http://dx.doi.org/10.13031/2013.23153.

Nash, J.E., Sutcliffe, J.V., 1970. River flow forecasting through conceptual models part I-a discussion of principles*. J. Hydrol. 10, 282–290. http://dx.doi.org/10.1016/0022-1694(70)90255-6.

Norton, M.R., Malinowski, D.P., Volaire, F., 2016. Plant drought survival under climate change and strategies to improve perennial grasses. A review. Agron. Sustain. Dev. 36 (2), http://dx.doi.org/10.1007/s13593-016-0362-1.

Oosterlo, P., Hofland, B., van der Meer, J.W., Overduin, M., Steendam, G.J., 2021. Calibration and preparation of field measurements of oblique wave run-up and overtopping on dikes using laser scanners. Coast. Eng. 167, 103915. http://dx.doi.org/10.1016/J.COASTALENG.2021.103915.

OpenCFD Ltd., 2019. OpenFOAM User Guide.

Ponsioen, L., van Damme, M., Hofland, B., Peeters, P., 2019. Relating grass failure on the landside slope to wave overtopping induced excess normal stresses. Coast. Eng. 148, 49–56. http://dx.doi.org/10.1016/j.coastaleng.2018.12.009.

SBW, 2012a. Wave Overtopping and Grass Cover Strength. Model Development. Report 120616-007, Deltares, Delft, The Netherlands.

SBW, 2012b. Wave Overtopping and Grass Cover Strength. Predictions of Prototype Tests. Report 120616-007, Deltares, Delft, The Netherlands.

Scheres, B., Schüttrumpf, H., Felder, S., 2020. Flow resistance and energy dissipation in supercritical air-water flows down vegetated chutes. Water Resour. Res. 56 (2), 1–18. http://dx.doi.org/10.1029/2019WR026686.

Slomp, R., Knoeff, H., Bizzarri, A., Bottema, M., De Vries, W., 2016. Probabilistic flood defence assessment tools. E3S Web Conf. 7, 1–14. http://dx.doi.org/10.1051/e3sconf/20160703015.

Steendam, G.J., Van Hoven, A., Van der Meer, J.W., Hoffmans, G., 2014. Wave overtopping simulator tests on transitions and obstacles at grass-covered slopes of dikes. Coast. Eng. Proc. 1 (34), http://dx.doi.org/10.9753/icce.v34.structures.79.

Suzuki, T., Altomare, C., Yasuda, T., Verwaest, T., 2020. Characterization of overtopping waves on sea dikes with gentle and shallow foreshores. J. Mar. Sci. Eng. 8 (10), 1–16. http://dx.doi.org/10.3390/jmse8100752.

Toimil, A., Losada, I.J., Nicholls, R.J., Dalrymple, R.A., Stive, M.J., 2020. Addressing the challenges of climate change risks and adaptation in coastal areas: A review. Coast. Eng. 156, 103611. http://dx.doi.org/10.1016/j.coastaleng.2019.103611.

Van Bergeijk, V.M., Verdonk, V.A., Warmink, J.J., Hulscher, S.J.M.H., 2021. The cross-dike failure probability by wave overtopping over grass-covered and damaged dikes. Water 13 (5), 690. http://dx.doi.org/10.3390/w13050690, URL: https://www.mdpi.com/2073-4441/13/5/690.

Van Bergeijk, V.M., Warmink, J.J., Frankena, M., Hulscher, S.J.M.H., 2019a. Modelling dike cover erosion by overtopping waves: The effects of transitions. In: Goseberg, N., Schlurmann, T. (Eds.), Coastal Structures 2019. Bundesanstalt für Wasserbau, Karlsruhe, pp. 1097–1106. http://dx.doi.org/10.18451/978-3-939230-64-9_110.

Van Bergeijk, V.M., Warmink, J.J., Hulscher, S.J.M.H., 2020a. Modelling of wave overtopping flow over complex dike geometries: Case study of the afsluitdijk. In: Coastal Engineering Proceedings. pp. 1–9. http://dx.doi.org/10.9753/icce.v36v.papers.52.

Van Bergeijk, V.M., Warmink, J.J., Hulscher, S.J.M.H., 2020b. Modelling the wave overtopping flow over the crest and the landward slope of grass-covered flood defences. J. Mar. Sci. Eng. 8 (7), 489. http://dx.doi.org/10.3390/jmse8070489.

Van Bergeijk, V.M., Warmink, J.J., Van Gent, M.R.A., Hulscher, S.J.M.H., 2019b. An analytical model of wave overtopping flow velocities on dike crests and landward slopes. Coast. Eng. 149, 28–38. http://dx.doi.org/10.1016/j.coastaleng.2019.03.001.

Van Damme, M., Ponsioen, L., Herrero, M., Peeters, P., 2016. Comparing overflow and wave-overtopping induced breach initiation mechanisms in an embankment breach experiment. E3S Web Conf. 7, 1–9. http://dx.doi.org/10.1051/e3sconf/20160703004.

Van der Meer, J., 2008. Erosion Strength of Inner Slopes of Dikes Against Wave Overtopping. Preliminary Conclusions After Two Years of Testing with the Wave Overtopping Simulator. Technical Report, Van Der Meer Consulting, Marknesse, The Netherlands.

Van der Meer, J.W., Hardeman, B., Steendam, G.J., Schüttrumpf, H., Verheij, H., 2010. Flow depths and velocities at crest and landward slope of a dike, in theory and with the wave overtopping simulator. Coast. Eng. Proc. 1 (32), 10.

Van der Meer, J.W., Snijders, W., Regeling, E., 2007. The wave overtopping simulator. In: Coastal Engineering 2006: (in 5 Volumes). pp. 4654–4666.

van Gent, M.R.A., 2021. Influence of oblique wave attack on wave overtopping at caisson breakwaters with sea and swell conditions. Coast. Eng. 164, 103834. http://dx.doi.org/10.1016/J.COASTALENG.2020.103834.

Van Hoven, A., Van der Meer, J., 2017. Onderbouwing Kansverdeling Kritisch Overslagdebiet ten Behoeve Van Het OI2014v4. Deltares, Delft, The Netherlands.

Van Hoven, A., Verheij, H., Hoffmans, G., Van der Meer, J., 2013. Evaluation and Model Development: Grass Erosion Test at the Rhine dike. Deltares, Delft, The Netherlands.

Warmink, J.J., Van Bergeijk, V.M., Frankena, M., Van Steeg, P., Hulscher, S.J.M.H., 2020. Quantifying the influence of transitions on grass cover erosion by overtopping waves. In: Coastal Engineering Proceedings 2020. pp. 1–8. http://dx.doi.org/10.9753/icce.v36v.papers.39.